


Evaluation of different keV-settings in dual-energy CT angiography of the aorta using advanced image-based virtual monoenergetic imaging

Martin Beeres¹  · Jesko Trommer¹ · Claudia Frellesen¹ ·
Nour-Eldin A. Nour-Eldin^{1,3} · Jan E. Scholtz¹ · Eva Herrmann² ·
Thomas J. Vogl¹ · Julian L. Wichmann¹

Received: 26 April 2015 / Accepted: 27 July 2015 / Published online: 2 August 2015
© Springer Science+Business Media Dordrecht 2015

Abstract To compare quantitative image quality in dual-energy CT angiography (DE-CTA) studies of the aorta using different virtual monoenergetic imaging (MEI) and advanced image-based virtual monoenergetic (MEI+) settings at varying kiloelectron volt (keV) levels. Fifty consecutive patients with clinically-indicated CT of the whole aorta to evaluate suspected aortic disease underwent DE-CTA on a third-generation dual-source CT scanner. Quantitative image quality indices were assessed. Contrast material, saline flush and flow rate were kept equal for

optimum comparability. DE-CTA MEI and MEI+ series ranging from 40 to 100 keV (10-keV intervals) were reconstructed. Signal intensity, noise, signal-to-noise ratio and contrast-to-noise ratio (CNR) of multiple aortic segments were evaluated. Comparisons between the different MEI and MEI+ datasets were performed. Three-hundred aortic segments total were evaluated. In the MEI+ series the 40, 50 and 100 keV MEI+ showed superior noise and CNR levels (+84, +58, +103 % on average; all $p < 0.05$) compared to MEI. However, signal intensity between MEI+ and MEI at nearly all aortic segments showed no significant difference ($p > 0.1$). MEI+ shows lower image noise compared to MEI, resulting in superior quantitative image quality, in particular at low keV levels (40 or 50 keV).

✉ Martin Beeres
beeres@gmx.net

Jesko Trommer
jeskotrommer@gmail.com

Claudia Frellesen
c.frellesen@gmail.com

Nour-Eldin A. Nour-Eldin
Nour410@hotmail.com

Jan E. Scholtz
jan.scholtz@gmx.de

Eva Herrmann
Herrmann@Med.Uni-Frankfurt.de

Thomas J. Vogl
T.Vogl@em.uni-frankfurt.de

Julian L. Wichmann
docwichmann@gmail.com

Keywords CT angiography · Aorta · Dual energy CT · Virtual monoenergetic imaging · Image noise

Introduction

Dual-energy computed tomography (DECT) has gained increasing acceptance particularly in contrast-enhanced CT due to its post-processing opportunities. These techniques have been previously used to enhance image quality, improve diagnostic accuracy, and reduce the amount of contrast material or radiation exposure [1–5].

Virtual monoenergetic images (MEI) can be derived using a post-processing technique which allows for calculation of images at a desired hypothetical energy (keV) level. These MEIs can be reconstructed at a wide range of keV levels from a single DECT study [6]. Previous studies have shown improved image quality with MEIs particularly at low keV levels due to increased iodine enhancement [4, 7]. By

¹ Department of Diagnostic and Interventional Radiology, Clinic of the Goethe University, Haus 23C UG, Theodor-Stern-Kai 7, 60590 Frankfurt, Germany

² Department of Biostatistics, Clinic of the Goethe University, Theodor-Stern-Kai 7, 60590 Frankfurt, Germany

³ Department of Diagnostic and Interventional Radiology, Cairo University Hospital, Cairo, Egypt

calculating MEIs at a low keV level close to the k-edge of iodine, vessel contrast can be substantially increased with this technique [8]. However, the established MEI technique suffered from a concurrent increase in image noise. Therefore, the lowest keV levels available (40 and 50 keV) were previously not recommended for clinical application with the existing MEI technique [9]. Recently, a noise-optimized MEI+ algorithm has been developed to improve image quality in contrast-enhanced DECT particularly at low keV levels [10].

Both algorithms (MEI and MEI+) are post-processing techniques that require a DECT Dataset acquired at two different tube voltage settings to allow for image decomposition [10]. Although DECT is subject of ongoing research, experience with the MEI+ algorithm is scarce [10–13]. Previous studies evaluating this technique in vascular DECT have shown promising results [12, 13], but its efficacy in imaging of the whole aorta has not been established so far.

Thus, the aim of our study was to evaluate the image quality of virtual MEIs using the established conventional MEI algorithm in comparison to the new noise-optimized MEI+ algorithm in DECT of the whole body aorta (DE-CTA).

Materials and methods

Patients and CT protocols

The study was performed as a single-centre, observer-blinded, retrospective study. The institutional review board approved this retrospective study. Data of primary unselected subsequent patients who underwent clinically-indicated thoraco-abdominal DE-CTA in arterial phase for assessment of the whole aorta were analysed (Table 1).

The study consisted of a patient cohort of 50 subsequent individuals who underwent thoraco-abdominal DE-CTA in

arterial contrast phase to rule out or evaluate various suspected or known aortic pathologies including aneurysm ($n = 27$), dissection ($n = 7$), endoleak following endovascular aneurysm repair ($n = 9$), bleeding ($n = 2$), and stent infection ($n = 1$). The indication for imaging was defined by the referring clinician from the vascular surgery or emergency department. Our patient cohort suffered from various underlying diseases which are summarized in Table 2.

Requirements for the DE-CTA examinations were age of at least 18 years, the ability to perform the examination with the necessary breath holds, and a valid clinical indication for CT angiography. Inclusion criteria for this study were image acquisition using DECT, sufficient image quality, and no deviations from the standard examination protocol. Exclusion criteria for this retrospective study were any deviations from the standard DE-CTA examination protocol, incomplete coverage of the whole aorta, and contrast medium administration malfunctions leading to insufficient vessel contrast.

A total of 50 patients (34 men, 16 women) were included, Table 3 gives an overview of the confirmed diagnoses of our patient cohort based on the DE-CTA examinations.

Image acquisition

All datasets were acquired on a 192-slice dual-source CT system (SOMATOM Force, Siemens Healthcare, Forchheim, Germany) in DECT mode. The examinations covered a region from the upper thoracic aperture to the inguinal ligaments to image the whole aorta.

Contrast enhancement was achieved by injecting a fixed amount of 90 mL of iodinated contrast material (iodine concentration of 400 mg/mL, Imeron 400, Bracco Imaging,

Table 1 Study population and evaluation of examination parameters

Parameter	Value
Patients	50
Male	34
Female	16
Age (years)	66 (37–86)
BMI (kg/m^2)	25.4 \pm 3.2 (18.6–31.3)
Scanning range (cm)	72.5 (43.5–88.2)
Scanning duration (s)	8.1 (4.8–9.7)
CTDI _{vol} (mGy)	4.9 (3.3–11.9)
Dose-length product (mGy cm)	344.4 (154–824)

Values in brackets indicate ranges

Table 2 Underlying clinical disease and co-factors in our study population

Disease	Patients (%)
Arterial hypertension	48 (96)
Diabetes mellitus	22 (44)
Coronary heart disease	20 (40)
History of myocardial infarction	14 (28)
COPD	11 (22)
Atrial Fibrillation	10 (20)
Uricaemia	8 (16)
History of cerebral ischemia	7 (14)
Obesity (BMI > 30)	6 (12)
Peripheral artery disease	6 (12)
Hypothyroidism	5 (10)
Renal insufficiency (Stage 1 or 2)	3 (6)

Table 3 Confirmed main diagnosis after CT examination

Diagnosis	Patients (%)
Abdominal aortic aneurysm (AAA)	14 (28)
Thoracic aortic aneurysm (TAA)	10 (20)
Endoleak post endovascular aneurysm repair (EVAR)	9 (18)
Stanford type A-dissection	5 (10)
Ruptured aortic aneurysm	3 (6)
No pathology on CT-examination	3 (6)
Stanford type B-dissection	2 (4)
Arterial bleeding	2 (4)
Infection of EVAR-stent-graft	1 (2)
Septic emboli	1 (2)

Milan, Italy) through a 18–20 G intravenous access on the patient's forearm at a flow of 4 mL/s using a double-syringe power injector (Injektron CT2, Medtron, Saarbruecken, Germany), followed by a 50 mL saline chaser bolus. Scan initiation was determined using bolus tracking software by placing a region of interest (ROI) in the descending thoracic aorta at the level of the pulmonary trunk after a trigger threshold of 140 Hounsfield units (HU) was reached.

DECT data were acquired with parameters as follows: pitch factor 0.7; collimation 192×0.6 mm; 90 kV/95 ref. mAs for tube A, Sn150 kV (with tin filter)/59 ref. mAs for tube B. Automatic exposure control was used in all groups (CAREdose 4D, Siemens Healthcare). All datasets were acquired in craniocaudal direction in deep inspiratory breath-hold throughout coverage of the whole aorta.

Image reconstruction

DE-CTA raw datasets were reconstructed using a medium sharp convolution kernel (B30f). The 90-kV and Sn150-kV images were then transferred to a multi-modality workstation (*Syngo.via* VA30A, Siemens Healthcare) equipped with dedicated software for the evaluation of DECT datasets (Dual Energy, Siemens Healthcare). MEI and MEI+ series were reconstructed using the same energy levels in 10-keV intervals ranging from 40 to 100 keV.

Images were reconstructed using a matrix size of 512×512 and 2 mm slice thickness with 2 mm increments.

Image analysis

As measures of objective image quality, several ROI measurements were performed by two radiologist with 4 and 5 years of experience in CTA on a regular PACS workstation (Centricity 4.2, General Electric Healthcare,

Dornstadt, Germany) using a circle tool with standard CTA windowing settings (center: 100 HU; width: 700 HU). Image noise [defined as standard deviation (SD) of the attenuation] was measured at the different defined anatomic landmarks on all MEI and MEI+ datasets. Furthermore, attenuation of the aorta at different anatomical levels (ascending aorta, descending thoracic aorta, abdominal aorta at the level of the celiac trunk, aortic bifurcation), the bilateral common femoral arteries, in the right and left ventricle, and in the pulmonary trunk were measured to determine the contrast enhancement. The ROIs within the arteries were maximized within the luminal diameter excluding the vessel wall and atherosclerotic plaques. Based on these measurements, the signal-to-noise ratio (SNR) of each region was determined according to the following equation: $SNR = \text{attenuation}/\text{image noise}$.

To calculate the contrast-to-noise ratio (CNR), we measured attenuation and SD of attenuation at the gluteus maximus muscle (ROI_{muscle}) compared with the attenuation of the aorta at the celiac trunk. CNR was calculated as $CNR = [(ROI_{\text{aorta}} - ROI_{\text{muscle}})/\text{image noise}]$. To minimise bias from single measurements, we calculated the average of four measurements for each ROI.

Radiation exposure

To estimate patient dose, we recorded the volume CT dose index ($CTDI_{\text{vol}}$ in mGy) as well as the dose-length-product (DLP in mGy cm) from the patient protocol, which is automatically generated for each examination and stored in the PACS of our department. All protocols were adjusted to similar kV/ref. mAs settings using automated dose control software (Table 1).

Statistical analysis

All statistical analyses were performed using dedicated software (Stata/IC 13.1, StataCorp LP, Texas, USA). Categorical variables were reported as counts. Continuous variables were expressed as median and range. For each variable, the Shapiro–Wilk-W-test was performed to investigate the normality of data distribution.

Differences in signal intensity, image noise, SNR and CNR between the datasets at different MEI and MEI+ keV levels were estimated with analysis of variance (ANOVA) for continuous normally distributed variables. The Bonferroni correction method was used to counteract the problem of multiple comparisons. Comparisons for non-normal distributed variables were performed using the Kruskal–Wallis test. A p value <0.05 was defined to be statistical significant.

Box plots were used to graphically represent medians and range of signal intensity, image noise, SNR and CNR.

Differences in ROI measurements between the both readers were assessed using Cohen's kappa (κ) interpreted in the following way: $\kappa < 0.20$, slight agreement; $\kappa = 0.21\text{--}0.40$, fair agreement; $\kappa = 0.41\text{--}0.60$, moderate agreement; $\kappa = 0.61\text{--}0.80$, substantial agreement; $\kappa = 0.81\text{--}1.0$, almost perfect agreement.

Results

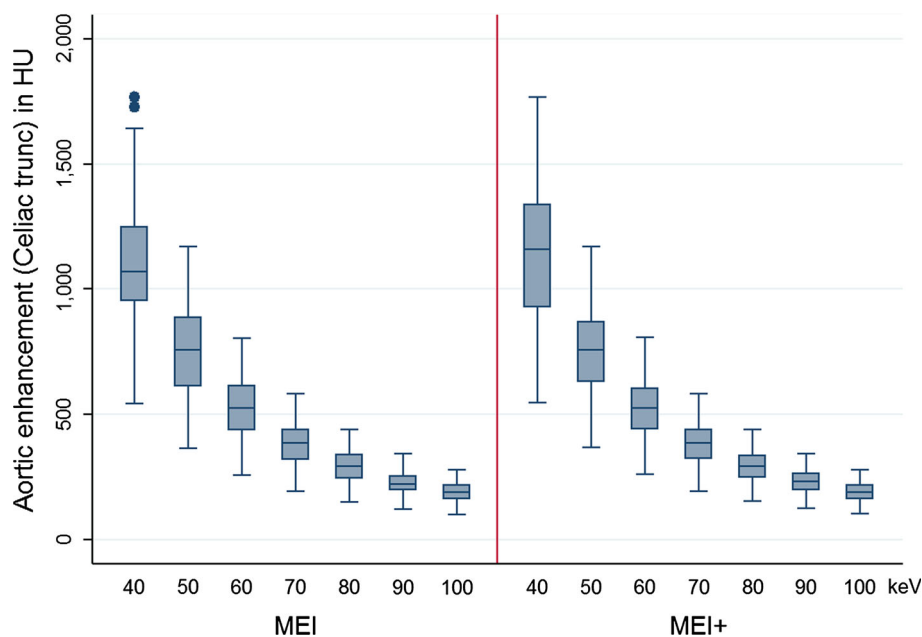
Image quality of all DECT examinations was considered diagnostic by the reading radiologist. Average CTDI_{vol} and DLP were 4.9 mGy and 344.4 mGy cm, respectively. A total of 300 aortic segments were evaluated with 1800 measurements in our study. Inter-reader agreement on ROI measurements was almost perfect ($\kappa = 0.88$).

In all investigated aortic segments, MEI and MEI+ showed a stepwise decrease in vessel attenuation as energies increased from 40 to 100 keV (Fig. 1; Table 4).

Using ANOVA comparison the intraluminal attenuation at each keV level showed to be independent of the used monoenergetic algorithm. There were no significant differences in attenuation between all measurements along the z-axis (Fig. 1).

In conventional MEI, image noise was lowest at 80 keV (20.1 ± 5.1 HU). In noise-optimized MEI+ the image noise was lowest at 100 keV (12.6 ± 2.2 HU). The image noise was higher in all MEI series compared to MEI+, the differences reached significance at 40, 50 and 100 keV ($p < 0.001$) (Table 5). Image noise was highest at 40 keV with both algorithms although it was significantly lower ($p < 0.001$) with MEI+ (61.5 ± 13.3 HU) compared to MEI (119.6 ± 39.2 HU) (Table 5).

Fig. 1 Comparison of aortic enhancement at the coeliac trunc. MEI = traditional virtual monoenergetic algorithm. MEI+ = advanced noise-optimized virtual monoenergetic algorithm



At 60 keV we observed a significant difference in image noise ($p = 0.014$) as well as CNR ($p = 0.023$), whereas SNR showed no significant difference ($p = 1.0$) (Table 5).

SNR was lower in all MEI compared to MEI+ except for the 70 and 80 keV reconstructions where SNR values were comparable (Table 5; Fig. 2). The differences in SNR showed statistical significance at 40, 50, 90 and 100 keV ($p < 0.001$) (Table 5). SNR was highest at 70 keV (15.8 ± 5.1 HU) with MEI and at 40 keV (15.9 ± 5.2 HU) with MEI+. Similarly, CNR was lower in MEI compared to MEI+, with significant differences at 40, 50 and 100 keV ($p < 0.001$) as well as 60 keV ($p = 0.023$) (Table 5; Fig. 3).

When comparing both groups individually, the MEI reconstructions at 70 keV showed the overall best image quality indices. The noise-optimized MEI+ reconstructions showed a nearly linear trend with a peak in objective image quality indices at 40 keV and a decrease with increasing keV levels (Figs. 2, 3, 4a, b). Overall, the 40 keV MEI+ reconstructions showed the overall best image quality indices (Figs. 2, 3).

Discussion

The aim of this study was to compare quantitative parameters of image quality between virtual MEI and MEI+ series reconstructed from DE-CTA examinations of the whole aorta performed on a third-generation dual-source CT system. While both algorithms resulted in similarly high intravascular attenuation values, the MEI+ technique showed significantly less image noise, especially at low keV levels (40 and 50 keV), ultimately resulting in

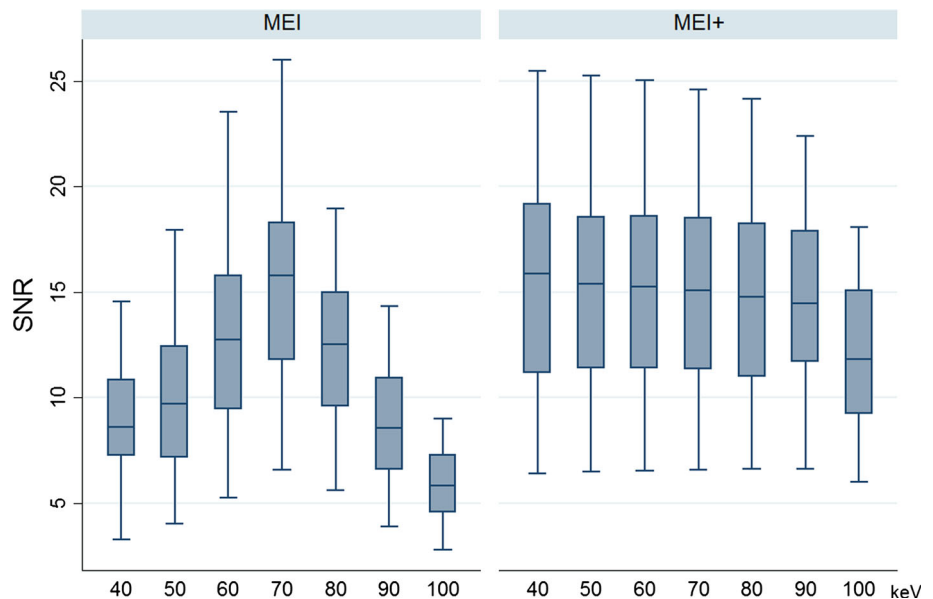
Table 4 Objective image quality parameters compared: median arterial attenuation at celiac trunk

Energy level (keV)	MEI	MEI+	<i>p</i> value
40	1070.9 (542.9–1764.6)	1160.3 (548.4–1767.6)	1.0/N.S.
50	758.0 (366.3–1169.0)	758.6 (370.8–1170.8)	1.0/N.S.
60	527.9 (258.9–806.7)	528.3 (262.7–807.3)	1.0/N.S.
70	385.9 (192.7–583.3)	386.2 (196.1–584.0)	1.0/N.S.
80	294.9 (150.1–440.1)	295.2 (153.4–440.6)	1.0/N.S.
90	223.7 (124.8–344.7)	233.7 (124.8–344.7)	1.0/N.S.
100	192.4 (102.4–278.4)	191.9 (104.9–278.6)	1.0/N.S.

Table 5 Image noise, signal-to-noise ratio (SNR), contrast-to-noise ratio (CNR)

Parameter (keV)	Noise (HU)		<i>p</i> value	SNR		<i>p</i> value	CNR		<i>p</i> value
	MEI	MEI+		MEI	MEI+		MEI	MEI+	
40	119.6 ± 39.2	61.5 ± 13.3	0.001	8.6 ± 3.3	15.9 ± 5.2	0.001	14.1 ± 7.6	33.3 ± 14.2	0.001
50	64.7 ± 22.9	42.2 ± 8.6	0.001	9.7 ± 3.7	15.4 ± 4.9	0.001	14.6 ± 6.4	28.4 ± 11.6	0.001
60	34.6 ± 13.3	29.5 ± 5.7	0.014	12.7 ± 4.7	15.3 ± 4.9	1.0/N.S.	18.7 ± 8.0	24.9 ± 9.6	0.023
70	21.6 ± 7.7	21.7 ± 3.8	1.0/N.S.	15.8 ± 5.1	15.1 ± 4.7	1.0/N.S.	20.8 ± 8.7	21.2 ± 8.1	1.0/N.S.
80	20.1 ± 5.1	16.7 ± 2.9	1.0/N.S.	12.5 ± 3.8	14.8 ± 4.8	0.15	14.9 ± 6.7	17.9 ± 6.9	1.0/N.S.
90	21.6 ± 5.2	13 ± 2.3	0.73	8.6 ± 2.9	14.5 ± 4.3	0.001	10.6 ± 4.5	14.9 ± 5.9	1.0/N.S.
100	26.1 ± 5.8	12.6 ± 2.2	0.001	5.8 ± 1.8	11.8 ± 3.5	0.001	6.3 ± 3.2	12.3 ± 5.0	0.001

Fig. 2 Comparison of SNR values between MEI and MEI+ reconstructions. MEI 70-keV series shows highest SNR values; a nearly linear decrease with increasing keV levels was observed for MEI+



superior objective image quality. Consequently, the optimal energy reconstruction levels for both techniques varied, as objective image quality indices with the MEI algorithm peaked at 70 keV while best results for the MEI+ algorithm were observed at 40 keV. Our results indicate that the recently introduced noise-optimized MEI+ technique should be preferably chosen over the

traditional MEI algorithm in DECT of the whole aorta to improve image quality.

To our knowledge, this is the first study to directly compare objective image quality indices between the MEI and MEI+ technique for imaging of the whole aorta. One important finding of our study is that there are no significant differences regarding the aortic enhancement (Fig. 1).

Fig. 3 Comparison of CNR values between MEI and MEI+. Highest CNR values were observed the MEI+ algorithm at 70 keV, with a linear decrease with increasing keV levels

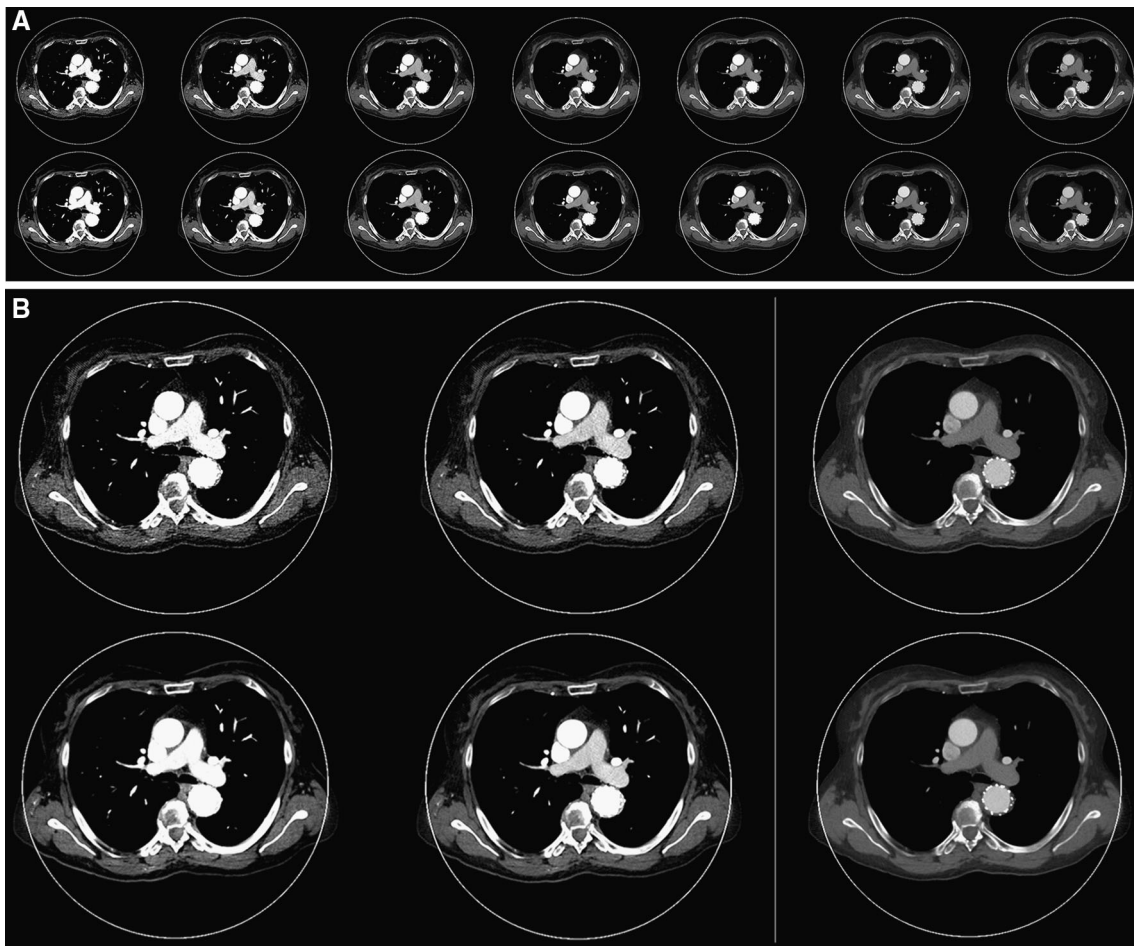
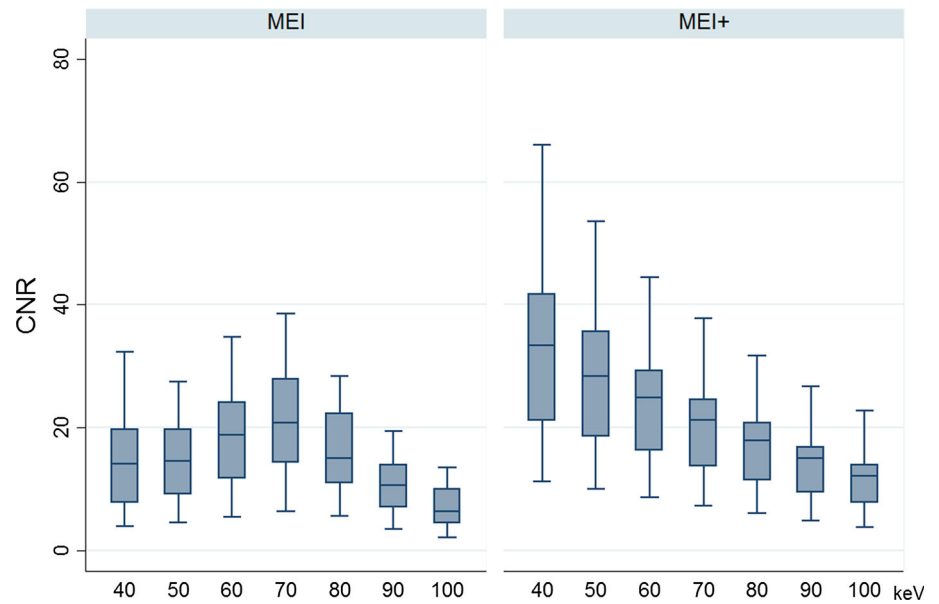


Fig. 4 **a** Upper row images show MEI reconstructions and lower row images show MEI+ reconstructions, both reconstructed at increasing keV levels ranging from 40 keV (left) to 100 keV with 10-keV

intervals. **b** Upper row images show MEI reconstructions and lower row images show MEI+ reconstructions at 40, 50, and 100 keV (from left to right)

Instead, the improvement in image quality is caused by significant differences in image noise between MEI and MEI+, particularly at the lower keV levels (40 and 50 keV). Grant et al. [10] first described the physical concepts behind the advanced image-based MEI+ algorithm which was developed to provide monoenergetic imaging at low keV levels without severe noise which was a limitation of the traditional MEI technique. The lower image noise levels with the MEI+ algorithm enabled the superior SNR and CNR values compared to the MEI algorithm in our study.

The increased intravascular attenuation at low keV levels is caused by reconstructing images with a virtual energy level closer to the k-edge of iodine (33 keV). This implicates a potential for imaging with a reduced contrast material bolus which has been previously demonstrated for the traditional MEI technique [14]. Nevertheless, additional studies are required to assess the usefulness of the MEI+ algorithm which may show superior image quality at low keV levels which provide strongest intravascular iodine attenuation.

Few previous studies have evaluated the traditional MEI technique for vascular DECT. Sudarski et al. [15] investigated MEI in DE-CTA for the evaluation of the abdomen and lower extremities. In their study, the abdominal vasculature showed superior image quality at 70 keV while the peripheral artery vessels revealed superior image quality in the 60 keV image dataset. Apfaltrer et al. [7] investigated low keV VMI (Virtual Monoenergetic Image) datasets for the evaluation of the pulmonary arteries. They found that the 70 keV dataset showed the highest CNR values with optimized contrast conditions superior to all other reconstructions. Both studies are in accordance with our results as we also found the best image quality parameters with the traditional MEI algorithm at 70 keV (Figs. 2, 3).

The MEI+ algorithm has shown an improvement in image quality mostly in phantom studies so far [10]. While evaluation of soft tissue structures in oncological DECT with reconstruction of MEI+ at 50 keV [11], vascular applications of this algorithm have consistently shown best results at 40 keV, especially in poor contrast conditions [12, 13]. Similarly, we observed optimal image quality at 40 keV (Figs. 2, 3; Table 5).

Our study suffers from certain limitations. First, all we used a retrospective study design to compare these both techniques. We included subsequent patients for the evaluation to mitigate potential patient-dependent bias. However, this prevented us from modifying the scan protocol to alter the tube voltage settings and we could not assess the potential of this technique for reduction of contrast material. This should be assessed in future prospective studies. Second, since we solely used a CT system and dedicated

post-processing from a single vendor, our results are vendor-specific. Although other vendors also provide MEI software, similar noise-optimized solutions with a focus on low-keV imaging are currently not available. Third, we arbitrarily chose keV settings with fixed intervals to provide a comprehensive analysis of the impact of varying keV levels and an upper limit of 100 keV as energy levels beyond this value can be expected to show insufficient vessel attenuation [16–18].

Conclusion

The results of our study based on a direct comparison of objective image quality of MEI and MEI+ reconstructions in DE-CTA of the whole aorta demonstrate that the noise-optimized MEI+ technique shows significantly lower image noise with comparable signal intensity, resulting in superior vascular contrast. Differences at low keV levels were particularly distinct as the best objective image quality was observed in 40-keV MEI+ series. One should be aware of the differences in optimal energy levels when performing MEI or MEI+ post-processing of aortic DE-CTA datasets.

Compliance with ethical standards

Conflict of interest The authors declare no conflict of interest.

References

- Carrascosa P, Capunay C, Rodriguez-Granillo GA, Deviggiano A, Vallejos J, Leipsic JA (2014) Substantial iodine volume load reduction in CT angiography with dual-energy imaging: insights from a pilot randomized study. *Int J Cardiovasc Imaging* 30(8):1613–1620. doi:10.1007/s10554-014-0501-1
- He J, Wang Q, Ma X, Sun Z (2014) Dual-energy CT angiography of abdomen with routine concentration contrast agent in comparison with conventional single-energy CT with high concentration contrast agent. *Eur J Radiol*. doi:10.1016/j.ejrad.2014.11.025
- Puryško AS, Primak AN, Baker ME, Obuchowski NA, Remer EM, John B, Herts BR (2014) Comparison of radiation dose and image quality from single-energy and dual-energy CT examinations in the same patients screened for hepatocellular carcinoma. *Clin Radiol* 69(12):e538–e544. doi:10.1016/j.crad.2014.08.021
- Sommer WH, Johnson TR, Becker CR, Arnoldi E, Kramer H, Reiser MF, Nikolaou K (2009) The value of dual-energy bone removal in maximum intensity projections of lower extremity computed tomography angiography. *Invest Radiol* 44(5):285–292. doi:10.1097/RLI.0b013e31819b70ba
- Park JH, Choi SI, Chun EJ (2012) Multidetector CT evaluation of various aortic diseases: diagnostic tips, pitfalls, and remedies for imaging artifacts. *Int J Cardiovasc Imaging* 28(Suppl 1):45–60. doi:10.1007/s10554-012-0071-z
- Yu L, Leng S, McCollough CH (2012) Dual-energy CT-based monochromatic imaging. *Am J Roentgenol* 199(5 Suppl):S9–S15. doi:10.2214/AJR.12.9121

7. Apfaltrer P, Sudarski S, Schneider D, Nance JW Jr, Haubenreisser H, Fink C, Schoenberg SO, Henzler T (2014) Value of monoenergetic low-kV dual energy CT datasets for improved image quality of CT pulmonary angiography. *Eur J Radiol* 83(2):322–328. doi:[10.1016/j.ejrad.2013.11.005](https://doi.org/10.1016/j.ejrad.2013.11.005)
8. Marin D, Boll DT, Mileto A, Nelson RC (2014) State of the art: dual-energy CT of the abdomen. *Radiology* 271(2):327–342. doi:[10.1148/radiol.14131480](https://doi.org/10.1148/radiol.14131480)
9. Sudarski S, Apfaltrer P, Nance JW Jr, Schneider D, Meyer M, Schoenberg SO, Fink C, Henzler T (2013) Optimization of keV-settings in abdominal and lower extremity dual-source dual-energy CT angiography determined with virtual monoenergetic imaging. *Eur J Radiol* 82(10):e574–e581. doi:[10.1016/j.ejrad.2013.04.040](https://doi.org/10.1016/j.ejrad.2013.04.040)
10. Grant KL, Flohr TG, Krauss B, Sedlmair M, Thomas C, Schmidt B (2014) Assessment of an advanced image-based technique to calculate virtual monoenergetic computed tomographic images from a dual-energy examination to improve contrast-to-noise ratio in examinations using iodinated contrast media. *Invest Radiol* 49(9):586–592. doi:[10.1097/RLI.0000000000000060](https://doi.org/10.1097/RLI.0000000000000060)
11. Albrecht MH, Scholtz JE, Kraft J, Bauer RW, Kaup M, Dewes P, Bucher AM, Burck I, Wagenblast J, Lehnert T, Kerl JM, Vogl TJ, Wichmann JL (2015) Assessment of an advanced monoenergetic reconstruction technique in dual-energy computed tomography of head and neck cancer. *Eur Radiol*. doi:[10.1007/s00330-015-3627-1](https://doi.org/10.1007/s00330-015-3627-1)
12. Bongers MN, Schabel C, Krauss B, Tsiflikas I, Ketelsen D, Mangold S, Claussen CD, Nikolaou K, Thomas C (2015) Noise-optimized virtual monoenergetic images and iodine maps for the detection of venous thrombosis in second-generation dual-energy CT (DECT): an ex vivo phantom study. *Eur Radiol* 25(6):1655–1664. doi:[10.1007/s00330-014-3544-8](https://doi.org/10.1007/s00330-014-3544-8)
13. Schabel C, Bongers M, Sedlmair M, Korn A, Grosse U, Mangold S, Claussen CD, Thomas C (2014) Assessment of the hepatic veins in poor contrast conditions using dual energy CT: evaluation of a novel monoenergetic extrapolation software algorithm. *RoFo: Fortschritte auf dem Gebiete der Rontgenstrahlen und der Nuklearmedizin* 186(6):591–597. doi:[10.1055/s-0034-1366423](https://doi.org/10.1055/s-0034-1366423)
14. Delesalle MA, Pontana F, Duhamel A, Faivre JB, Flohr T, Tacelli N, Remy J, Remy-Jardin M (2013) Spectral optimization of chest CT angiography with reduced iodine load: experience in 80 patients evaluated with dual-source, dual-energy CT. *Radiology* 267(1):256–266. doi:[10.1148/radiol.12120195](https://doi.org/10.1148/radiol.12120195)
15. Sudarski S, Apfaltrer P, Nance JW Jr, Schneider D, Meyer M, Schoenberg SO, Fink C, Henzler T (2013) Optimization of keV-settings in abdominal and lower extremity dual-source dual-energy CT angiography determined with virtual monoenergetic imaging. *Eur J Radiol* 82(10):e574–e581. doi:[10.1016/j.ejrad.2013.04.040](https://doi.org/10.1016/j.ejrad.2013.04.040)
16. Ippolito D, Talei Franzesi C, Fior D, Bonaffini PA, Minutolo O, Sironi S (2015) Low kV settings CT angiography (CTA) with low dose contrast medium volume protocol in the assessment of thoracic and abdominal aorta disease: a feasibility study. *Br J Radiol* 88(1049):20140140. doi:[10.1259/bjr.20140140](https://doi.org/10.1259/bjr.20140140)
17. Komatsu S, Kamata T, Imai A, Ohara T, Takewa M, Ohe R, Miyaji K, Yoshida J, Kodama K (2013) Coronary computed tomography angiography using ultra-low-dose contrast media: radiation dose and image quality. *Int J Cardiovasc Imaging* 29(6):1335–1340. doi:[10.1007/s10554-013-0201-2](https://doi.org/10.1007/s10554-013-0201-2)
18. Siegel MJ, Schmidt B, Bradley D, Suess C, Hildebolt C (2004) Radiation dose and image quality in pediatric CT: effect of technical factors and phantom size and shape. *Radiology* 233(2):515–522. doi:[10.1148/radiol.2332032107](https://doi.org/10.1148/radiol.2332032107)